AUTHOR	Kasvi Elina, Saarinen Aino, Kämäri Maria, Porkka Jutta, Alho Petteri, Ekholm Petri
TITLE	The effect of seasonal variation, flow conditions and erosion forces on suspended matter fluxes from boreal gypsum-treated agricultural fields
YEAR	2024
DOI	https://doi.org/10.1016/j.catena.2024.108199
VERSION	Author's accepted manuscript
COPYRIGHT	CC-BY-NC-ND
CITATION	Kasvi, E., Saarinen, A., Kämäri, M., Porkka, J., Alho, P., Ekholm, P., 2024. The Effect of Seasonal Variation, Flow Conditions and Erosion Forces on Suspended Matter Fluxes from Boreal Gypsum-Treated Agricultural Fields. CATENA 243, 108199. doi: 10.1016/j.catena.2024.108199.

The effect of seasonal variation, flow conditions and erosion forces on suspended matter fluxes from boreal gypsum-treated agricultural fields

Kasvi, Elina[1] (corresponding author) Saarinen, Aino[1]; Kämäri, Maria[2]; Porkka, Jutta[1]; Alho, Petteri[1]; Ekholm, Petri[2].

1. University of Turku, Department of Geography and Geology. 20014 Turun Yliopisto. (elina.kasvi@utu.fi)

2. Finnish Environment Institute, Marine and freshwater solutions, Latokartanonkaari 11, 00790 Helsinki, Finland

Abstract

Like many other bodies of water, the Baltic Sea is facing a severe eutrophication problem, the excessive nutrient load currently originating primarily from agriculture. Gypsum treatment has shown promising results in reducing phosphorus and suspended sediment loads, especially in fine-textured soils, but its efficacy has not been investigated on catchment scale to any wide extent. This study examines the functionality of the gypsum treatment in an agriculture-dominated boreal catchment in the Archipelago Sea basin. The relation between turbidity and hydro-climatological factors was analysed during different years and seasons and the effect of stream erosion during different flow stages was investigated by applying 2D hydraulic modeling. A special focus was given to deviating winter conditions and freeze-thaw cycles.

The results highlight the dependency of stream water turbidity on the discharge and the potential negative impact of the climate change-altered winter conditions of the hemiboreal climate zone on gypsum treatment effectiveness. The turbidity increased even more during high winter discharges, compared to other seasons suggesting that the more frequent freeze-thaw cycles and precipitation coming as rain during the unvegetated period increase erosion challenging the gypsum efficacy. Modelling results revealed that the increased erosional power during very high discharges caused settled material resuspension or stream bed or bank erosion leading to a cumulative increase in turbidity at downstream, an issue needing further research. Demonstrating the real and long-term effects of nutrient reduction measures requires catchment scale investigations over years, considering climatological factors. Based on this study, local and short-term investigations can potentially lead to over-simplified interpretations.

Keywords: gypsum treatment, agriculture, phosphorous, Baltic Sea, eutrophication, erosion

1. Introduction

The state of our water resources, including the water quality and aquatic ecosystems, and the unpredictable impacts of climate change on the hydrological cycle, has become a severe global concern and many national and international initiatives to ensure cooperation and joint responsibility and to create a framework for water protection have been established. For example, the EU Water Framework Directive (WFD) and the EU Marine Strategy Framework Directive (MSFD, Marine Directive) are guidelines aiming to ensure systematic criteria and methodological standards in water protection across Europe.

One of the main global problems related to coastal waters is agriculture-originated eutrophication, which has been aggravating for decades due to the demands of the growing population (Tilman et al., 2001; Paerl and Paul, 2012), and is exacerbating due to climate change effects, especially on the boreal areas (Paerl and Paul, 2012; Wang et al., 2020; Pavlidou et al., 2024). Economical and effective procedures to control eutrophication have been sleeked and studied for decades (e.g. Higgins et al., 1976; Verduin 1969; Vitousek et al., 2009). However, there is still an identified need to understand the sources of nutrient loads and possible solutions for their mitigation as well as in catchment scale investigation of the functionality of the measures (Vigouroux & Destouni, 2022).

Gypsum ($CaSO_4 \cdot 2H_2O$), used for centuries in soil improvement, has been increasingly used as a measure to fight against eutrophication, especially in agriculture-dominated catchments (Zhu and Alva, 1994; Uusitalo et al., 2012; Kost et al., 2018; King et al., 2016). Unlike agricultural lime, gypsum readily dissolves in soil forming divalent calcium and sulfate ions, enhancing soil solution ionic strength (Appelo and Postma 2005). This process promotes microaggregation of the smallest soil particles potentially strengthened by calcium bridges, thereby reducing erosion and erosion-related particulate phosphorus load especially in fine-textured soils (Shainberg et al., 1989; Uusitalo et al., 2012; Ollikainen et al., 2020). As the functionality of gypsum is directly linked to preventing soil erosion, the efficacy of the gypsum amendment can be approached by investigating the variations of stream water turbidity and suspended sediment load, which are expected to increase with warmer and wetter winters (Ekholm et al., 2024; Salmela et al 2022)

On top of the operating principle of gypsum, not much is known about its effectiveness in phosphorus reduction in catchment scale or its dependency of prevailing environmental factors. Given the increased ionic strength of not only soil solution but also runoff, it is possible that the particles also aggregate in the stream and settle on the river bed during low flow velocities resuspend during high flows reducing the long-term effect of the gypsum amendment, and the performance of gypsum in the areas with varying flow velocities (Ekholm et al., 2024). However, as the contribution of fluvial erosion at the stream bed and banks to the material fluxes relative to diffuse loadings during extreme events are poorly understood, it is difficult to assess the functionality of gypsum. Pietiläinen and Ekholm,

(1992) found 90% of suspended sediments transported by an agricultural stream in SW Finland to originate from surface soil rather than stream bank. On the other hand, Gellis & Noe (2013) stated that stream bank erosion can contribute with similar magnitude as agricultural land to the annual fine-grained suspended sediment load. More research is needed to elucidate the potential for resuspension of gypsum-treated material from the streambed during high flows.

In addition, no study thus far has investigated gypsum treatment efficacy and its dependency on seasonal environmental and climatological factors in a catchment scale. This study takes an important step toward catchment scale investigation of gypsum as a nutrient reduction measure and its dependency on seasonal variations, erosion forces, and flow conditions by exploiting the potential of long-term spatial monitoring data combined with computational modelling. The study is based on a pilot executed in the catchment of Archipelago Sea, southwest Finland, where two agricultural sub-catchments were amended with gypsum as part of the Water Protection Program by the Finnish Ministry if Environment with an aim to reduce phosphorus loads to the Baltic Sea and monitored continuously for 5 years (Ministry of Environment, 2024; ELY, 2024). During an extreme winter flood in 2020, the gypsum amendment provided conflicting results as the response of the other treated areas to the gypsum amendment decreased notably (Ekholm et al., 2024). Our hypothesis is that the gypsum could have been settled on the stream bed during low to medium-sized floods, but resuspended at high floods, encountered in winter 2020.

We utilize comprehensive monitoring records of water quality and quantity, weather, land cover and topographic data, and two-dimensional hydraulic modeling of erosional power to seek reasons for the variability in the turbidity level in the two treated areas. We link the measured turbidity level with discharge, seasonal environmental variation, and erosion power during different flow stages.

2. Case study at Savijoki: a small agricultural catchment

The study site is located in the catchment of the Archipelago Sea, a Northern sub-basin of the Baltic Sea, which suffers from severe eutrophication mainly caused by agricultural activities within its intensively cultivated catchment in Southwestern Finland (Räike et al., 2020; Rankinen et al., 2016). The area falls within the hemiboreal climate zone, characterized by distinct seasons, with climate change exacerbating eutrophication and oxygen loss (Arheimer et al., 2012; Huttunen et al., 2021). Winters are projected to experience the strongest warming and precipitation increases, potentially amplifying sediment yields from watersheds, especially outside the vegetation period when soil is more susceptible to erosion (Salmela et al., 2022). Recognizing the accelerating impact of climate change on eutrophication, reducing nutrient loads from the catchment is crucial.

A gypsum treatment pilot was executed in the valley of the River Savijoki, in Southwest Finland during 2016–2020 (Fig. 1a). The 28 km long river is a tributary of the River Aurajoki discharging into the Archipelago Sea. The Savijoki has eroded itself into a several-meters-deep valley that meanders across an old agricultural landscape where active cultivation dominates the land use still today. The average slope of the fields ranges from 0.8% to 2.4%. The ecological state of Savijoki is defined as poor, which is the second lowest category in a 5-level classification (SYKE, 2022).

During the study period (2016-2020) the mean temperature at the closest meteorological site (Turku Airport) was 6.4 °C, while the mean long-term temperature was 5.5 °C (years 1971–

2020). Normally, the wintertime air temperatures remain under zero, the coldest month being February (FMI, 2022). In the inland areas of Southwest Finland, the thermal growing season typically begins in the last week of April. Therefore, during the winter period (Jan. 1st to May 15th), some fields are without protective vegetation cover and intensively tilled in the study area.

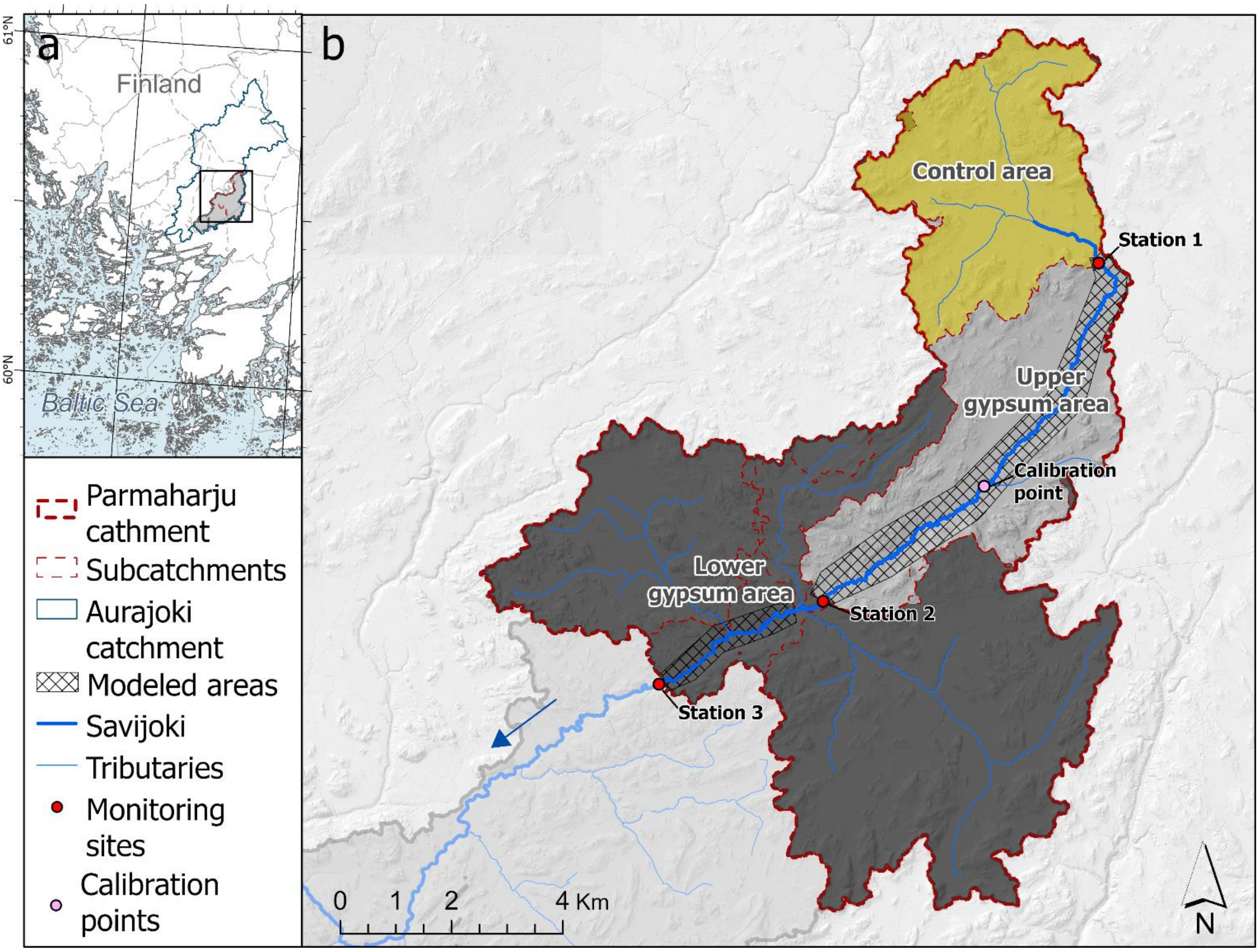

Fig .1. The study area. a) The agricultural Parmaharju catchment is part of River Savijoki, which is a tributary of River Aurajoki, ultimately discharging into the Baltic Sea. b) The pilot site consists of three sub-catchments: the control area, and the upper and lower gypsum areas. Locations of monitoring sites (Stations 1, 2, and 3) and the calibration point are marked in the figure. The control site had no gypsum treatment. Gypsum was spread over *upper and lower gypsum areas in autumn 2016 to reduce agricultural nutrient losses, particularly phosphorus.*

The mean long-term precipitation in the area is 655 mm which is almost the same as during the study period (642 mm), with 19% of precipitation coming as snow. The winter period is characterized by low precipitation levels, compared to other seasons. Discharge and turbidity peaks occur usually during autumn due to rain and during spring due to snow melt. During early winter (Jan-March) discharges and turbidity levels are typically below the annual average as soil frost and snow cover prevent soil erosion. Early winter high discharges are still? rare, as the temperatures remain under zero.

The pilot reach is 21 km long and has a catchment area of 81.3 km^2 (Fig 1b). The discharge at the upstream of the reach (Station 1 in Fig. 1) varies normally between 0.1 and 2.5 m^3/s, the mean turbidity being 116 FNU (Skarbøvik et al., 2023). In the study setting, the catchment was further divided into three sub-catchments the control site, the upper gypsum area, and the lower gypsum area (Fig. 1b). During the study period, turbidity was measured in three Stations to examine the gypsum treatment efficacy (Stations 1-3). It must be noted that the control area affects the water quality also at Station 2 and Station 3 is affected by the whole watershed consisting of the control area, and upper and lower gypsum areas. The land use of the drainage areas discharging via Stations 2 and 3 are comparable to each other's, while the control area (i.e. Station 1) has slightly smaller proportion of agricultural fields and more forests (Table 1). The monitoring started in February 2016 and gypsum treatment was executed in autumn 2016. Thus, the winter and summer 2016 represent gypsum free conditions. Out of the agricultural fields in the control site and upper gypsum area (total field area 1465 ha) 28 % were treated (Table 1), while out of the fields of the entire drainage area (total field area 3481 ha), 42 % were treated.

Table 1. Characteristics of the drainage areas. Station 1 is located at the outlet of the control area. Station 2 collects water from the control area and upper gypsum area while Station 3 covers the entire drainage basin. The soil types were derived from the Finnish Soil Database. Natural Resources Institute Finland and Geological Survey of Finland (Lilja et al., 2009). *Land use data from the year 2012 was retrieved from the Coordination of Information on the Environment (CORINE) with 20 m resolution.*

	Station 1	**Station 2**	**Station 3**
Drainage area (ha)	1500	3260	8120
Agricultural fields (m^2)	585	1465	3481
Fields treated with gypsum (%)	0	28	43
Land use %			
Agricultural fields	39	45	43
Forest	56	48	51
Urban	4	6	5
Other	1	0	1
Soil type %			
Fine-grained soil (of which clay)	44	49	49
Rock	37	32	33
Glacial till	14	13	12
Sand	4	6	5
Peat	1	0	1

The turbidity and runoff of the areas were monitored before and after the gypsum amendment. Based on the same monitoring data, Ekholm et al. (2024) showed that, before the gypsum spreading, the suspended solids and particulate P losses from the gypsum areas were approximately 30% larger than from the control area. A source apportionment on riverine turbidity suggested that, after the gypsum treatment, the particulate P losses from upper and lower gypsum areas were on average 72% and 19 % lower than from the control area, respectively. Based on the results of Ekholm et al. (2024), the early winter period of 2020 was unusual with particularly high discharge especially in February (Fig. 2). The period was also characterized by warm temperatures and high loss of particulate P, the lower gypsum area having an even higher P loss compared to the upper area. The question thus is what caused the big difference in the responses of the two gypsum areas.

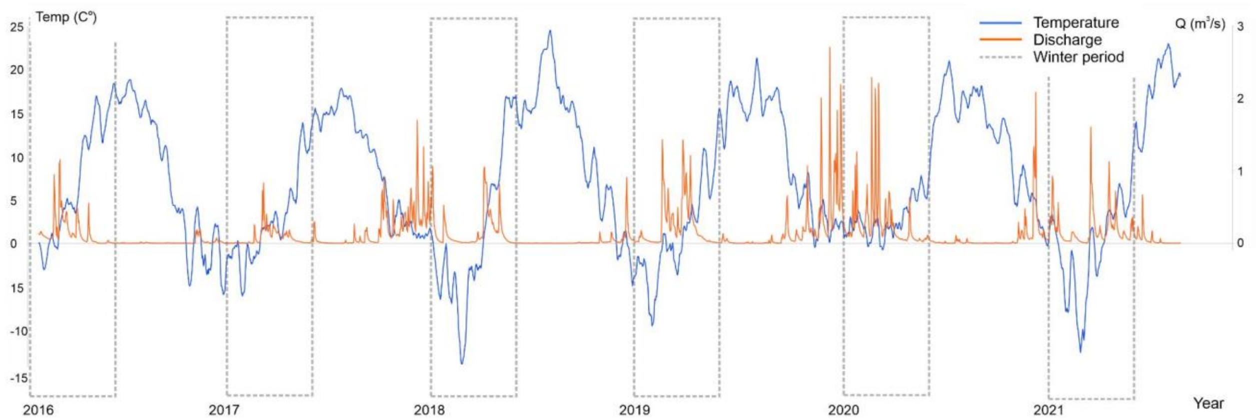

Fig. 2. Temperature and average daily discharge at Station 1 during 2016–2021, after the gypsum spreading. The winter seasons are highlighted with dashed lines. Winter 2020 differs from other winters with higher discharges and temperatures.

3. Data and methods

3.1. Data collection

3.1.1 Flow magnitude

Hourly runoff was measured at the outlet of the control area by a calibrated V-notch weir, and water-level measurements (Station 1, Fig. 1). The hydrological station was managed by the Southwest Finland Centre for Economic Growth, Transport and the Environment (Ekholm et al., 2024). In addition, water surface elevation was measured hourly at two other monitoring stations located at the outlet of the upper gypsum area (Station 2) and the lower gypsum area (Station 3) (Fig. 1). Water surface elevations were measured with VRS-GNSS at the calibration point. In addition, drone flights were executed in winter 2023, to monitor a flood extent, which was used in model validation.

3.1.2. Water quality monitoring

In situ hourly water quality monitoring was carried out during 2016 – 2020 in the three monitoring sites (Fig. 1). YSI EXO2 sonde equipped with a central wiper brush was used to measure water temperature and turbidity in each site. The high frequency in situ monitored turbidity can be used to indicate the level of particulate P (Kämäri et al., 2020) or suspended solids concentration (Skarbøvik et al., 2023) in case a good correlation exists between the variables. The Savijoki catchment fields are clay-dominated and the coefficient of determination (R^2=0.87) between turbidity and suspended solids is high (Skarbøvik et al. 2023). Over 80% of the P transported by the River Savijoki is attached to the soil particles.

The sensors were cleaned regularly and calibrated in a laboratory every six months. Reference water samples were collected three to five times monthly during wet periods and once a month during low flow periods. Low flows appear typically during the summer season and in cold winters. Turbidity was analysed from the water samples in an accredited laboratory and used to verify the monitoring data.

Analysis of covariance and Pearson's correlation was used to test the differences in the relationship between turbidity levels and discharge at the sites. Statistical analyses and tests were performed using proc glm of the Statistical Analysis System (SAS) software package, version 8.2.5 SAS Institute Inc., Cary, NC, USA.

3.1.3 Open source environmental data

Daily hydro-climatological data (precipitation, ground frost, and temperature) during 2016–2020 was derived from the WSFS of the Finnish Environment Institute (Huttunen et al., 2016; Vehviläinen and Huttunen, 2001). The WFSF combines observations and forecasts to simulate the water cycle in Finnish and bordering catchment areas. The model is used for simulating and forecasting hydrological variables, for example, the water levels and discharges for lakes and rivers, groundwater levels, and snow water equivalent. The daily data represents mean values over the entire Savijoki catchment (130 km^2). Ground frost estimates are computed separately for open, forest, and peat areas. Open-area soil frost estimates were used to best describe the frost situation in fields.

3.2. Computational modelling

3.2.1. Defining the model boundaries

Two-dimensional hydraulic models were built to simulate the inundation area and distribution of the erosional forces during three flow stages: mean discharge (MQ), mean high discharge (MHQ), and high discharge (HQ). The aim of the modeling was to figure out how the flow stage affects the flood extent and erosional forces in both areas and if there are major differences between the areas. We investigated the connectivity of the river system and the potential of the aggregated material to resuspend from the stream storage during high flows. The upper and lower gypsum areas were modelled separately.

For the upstream boundary of the upper gypsum area, MQ, MHQ, and HQ discharges at Station 1 (Fig 1) were defined based on the continuous discharge data of the monitoring period 2016–2023 (Table 2). As the tributaries add to the flow magnitude along the upper gypsum area, discharge was measured also at the main tributaries during various flow stages and the input from the tributaries was considered in the model. Next, the MQ, MHQ, and HQ values were defined for the upstream boundary of the lower gypsum area (i.e. Station 2): as there was only water level monitoring at Station 2, discharge was measured in situ during five different events and the discharge rating curve was formed using a regression curve between the *in situ* discharge measurements and continuous WSE monitoring data. The MQ, MHQ, and HQ at Station 2 were then calculated from the resultant discharge rating data. Next, experienced? flow events which represent MQ, MHQ, and HQ at Station 1 were identified and the water levels at Station 2 during those events were extracted and used as downstream boundary conditions for the upper gypsum area. Similarly, the MQ, MHQ, and HQ events were identified from the discharge rating curve at Station 2 and the corresponding water level value at Station 3 was used as the downstream boundary of the lower gypsum area.

The model geometries were built using a Digital Elevation Model (DEM) with a 2 m cell size, produced by the National Land Survey of Finland supplemented, with bathymetric measurements on the field during the summer of 2022. The bathymetric data was collected with a Sontek River Surveyor S5, which is an Acoustic Doppler Current Profiler (ADCP) equipped with sonar. Trimble VRS-GNSS (Virtual reference station Global Navigation Satellite System) was used for data collection on very shallow or rocky areas.

Table 2. *The discharge (Q) of the three flow stages MQ, MHQ and HQ in the upper and lower gypsum areas.*

	Upper area [m^3/s]	Lower area [m^3/s]
MQ	0.16	1.2
MHQ	2.33	7.02
HQ	4	20.5

3.2.2. Building the model

The 2D flow simulations were conducted using HEC-RAS 2D (version 6.3.1), which is an open, physically-based hydraulic modeling software (Hydrologic Engineering Center, 2023). The research area was divided into two modelling domains, namely, the upper and lower gypsum areas. An altering mesh was used, with cell sizes varying between 1 m at the stream to 3m on the catchment area. The horizontal length of the modelled river reaches in the upper and lower gypsum areas were 10.7 km and 3.4 km with 5.5 m and 4.7 m elevation differences, respectively. Thus, the upper area has a smaller average slope (0.0514 %) compared to the lower one (0.1382 %).

A vector format land use layer covering the modelling domain with higher detail than CORINE was created based on aerial photographs and field observations. The land use layer was used to define spatially varying Manning's bed roughness coefficients for the reach. Initial Manning's values were estimated following a guide constructed by H. Barnes (Barnes, 1967). Standard Shallow Water Equations, simplifications of Navier-Stokes equations, were utilized and solved using the Eulerian-Lagrangian Method (ELM-SWE). Incompressible flow, uniform density, and hydrostatic pressure are assumed, and the equations are Reynolds averaged so that turbulent motion is approximated using eddy viscosity. They apply to environments where vertical velocity is small, and pressure is hydrostatic.

It must be noted that the stream and the flow magnitude are small compared to the catchment area and length of the modelling reach. In addition, the model was built partly based on estimated discharge values. That's why the modelling results must be treated as indicative.

3.2.3 Calibrating, validating, and running the model

Separate *in situ* field measurements of discharge and water level along the stream were performed for model calibration and validation (See Fig. 1). The model calibration was done for the upper gypsum area by adjusting Manning's roughness values according to the land use. Data based on flow conditions with discharge of 0.5 m^3/s at Station 1 on April 11th, 2023 (Table 3). These conditions represent the hydraulic behavior of the reach after a usual rain event (compared to MQ=0.16m^3/s). The modelling time step was set to 3 seconds, and a period of 14 hours was modeled for the upper gypsum area. The Manning's roughness values were adjusted in the calibration process to achieve the measured water surface elevation at the calibration point (point 3). As the modelling reach was long, and had high vertical change, a difference up to 0.1 m was accepted in the calibration. When the modelled WSEs were considered corresponding to the measured ones, the calibration was finished. The final Manning's roughness values are presented in table 4. After adjusting the roughness values for the upper area model, the same values were used for the lower gypsum area based on its land use. The lower area was not calibrated separately, as the river is difficult to access along the lower reach: there are no roads, paths, or other means of access and the land is privately owned. The lack of calibration data adds to the insecurities of the modelling results.

Table 3. Calibration and validation values of the upper and lower gypsum areas and the corresponding modelled values. The lower gypsum area model was validated with an aerial photograph of the inundated area.

	Upstream BC	**Measured WSE (m)**	**Modelled WSE (m)**	**Downstream BC**

Upper gypsum area	Q (Station 1)	Calibration point	Calibration point	WL (Station 2)
Calibr (4/2023)	0.5	36.62	36.72	30.8
Valid (1/2023)	1.8	37.27	37.20	31.29

Lower gypsum area	Q (Station 2)			WL (Station 3)
Valid (1/2023)	6.48	Model validated with flood extend from aerial image		19.04

For model validation, we used *in situ* field measurements taken on January 17, 2023, when the discharge at Station 1 was 1.8 m^3/s, somewhat below the MHQ of 2.33 m^3/s. The model validation was done for both upper and lower gypsum areas, separately. At the upper area, the modelled WSE at point 3 was compared to the measured one (Table 3). The lower gypsum area was validated by comparing the modelled flood extent to the actual flood extent, extracted from a drone-based orthoimage taken during the event.

Table 4. The final Manning's roughness values (n) *were used in computational modelling of the upper and lower gypsum areas.*

Description	**n**
slightly vegetated/ open stream/agricultural field	0.03
vegetated stream	0.035
rocky or forrested stream	0.06

After the model validation, the three flow situations, i.e MQ, MHQ and HQ were simulated for both gypsum areas (Table 2). Steady state models of 14 hours were modelled with 3 seconds time step for both gypsum areas. From the modelling results, the flow depth, velocity, and inundated area were extracted and analysed.

4. Results:

4.1. Seasonal turbidity variation

During the entire measurement period, the turbidity levels in the area were highest during autumn periods (~100 FNU) which is typical for the boreal environments, while the wintertime (1st Jan - 15th May) and summer time mean turbidities stayed around 70 and 40 FNU, respectively (Fig 3). However, the average turbidity of winter 2020 (>130 FNU) was even higher than the average autumn level, with February 2020 being exceptional (Table 5). The turbidity correlated strongly with discharge and precipitation coming as rain during autumn and winter periods, but not that much during the summer. The correlation between turbidity and discharge was strongest during autumn, while the correlation between turbidity and rain was strongest during winter. As the wintertime high discharges may originate from snow melt or rain, it is possible that the snow melt induced high flows do not affect turbidity to same extent than rain. Before gypsum application, the mean winter turbidity in Stations 2 and 3 was larger than in Station 1 (Table 1), which was expected due lower percentage to agricultural fields in the control area. After gypsum application the turbidity in the Stations 2 and 3 decreased to a similar level compared to Station 1, and the correlation between turbidity and discharge weakened. This indicates that gypsum had reduced the wintertime soil erosion the fields. However, in winter 2020, the treated areas (Stations 2 and 3) had much higher turbidities compared to Station 1 and the turbidity of the lower gypsum area (Station 3) were notably higher compared to the upper gypsum area (Station 2) (Table 5). Then, the turbidity also correlated strongly with discharge, like before the gypsum treatment.

Table 5. The average turbidities during different seasons in each measurement station during 2016-2021 and the Pearson correlation of turbidity with discharge and precipitation sum

from past 10 days. The pre-gypsum turbidity (winter 2016) and winter 2020 with extremely high turbidities are calculated separately.

Mean FNU			
Winter (pre-gypsum)	56,34	74,63	70,10
Winter (with gypsum)	60,62	64,89	64,12
Winter 2020	132,53	156,29	166,56
Feb 2020	191	246	305
Summer (with gypsum)	36,30	35,24	38,58
Autumn (with gypsum)	100,95	106,70	104,81
r (FNU vs Q)			
Winter (pre-gypsum)	0,63	0,88	0,87
Winter (with gypsum)	0,63	0,63	0,67
Winter 2020	0,86	0,90	0,92
Summer (with gypsum)	0,58	0,56	0,50
Autumn (with gypsum)	0,77	0,81	0,82
r (FNU vs. rain)			
Winter (pre-gypsum)	0,37	0,25	0,31
Winter (with gypsum)	0,46	0,50	0,51
Winter 2020	0,50	0,58	0,64
Summer (with gypsum)	0,37	0,47	0,48
Autumn (with gypsum)	0,57	0,60	0,60

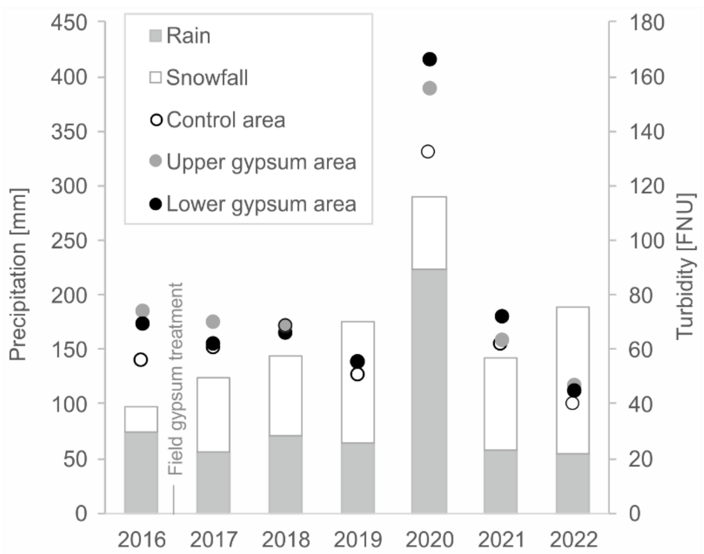

Fig. 3. Variation of precipitation and turbidity in the study areas during wintertime. The pillars represent the cumulative precipitation of rain and snowfall in the Savijoki catchment

area during the winter seasons (1st Jan - 15th May). Mean arithmetic turbidity during winter periods (monitoring started Feb 2nd 2016) in the control area, and the lower and upper gypsum areas are presented by dots.

4.2. Effect of varying winter conditions on turbidity

To get a deeper insight to the reasons causing the winter 2020 turbidity peak, the dependency of turbidity on varying winter conditions (air temperature, soil frost, and discharge) was analysed by comparing winters 2016-2022 to winter 2020. During the winter period (with temperatures increasing towards April and May), the highest turbidities were linked to temperatures between 0 and 5 degrees, although temperatures ranging from -20 to +20 °C are common (Fig 4a). The more the temperature fell below zero, the lower the turbidity. The winter of 2020 lacked cold temperatures, while temperatures between 0 and 5 were over-presented. Also in 2020, the highest turbidity peaks occurred simultaneously with temperatures around 5 degrees.

Figure 4b describes the maximum depth of the soil frost and its relation to turbidity. It must be noted that the surface soil may not be frozen while there still exists frost in the deeper soil layers. The soil frost went hand in hand with temperature: during the winters of 2016–2012, the frost depth of 10 to 15 cm was common, sometimes reaching 20 cm (Fig 4b). During the winter of 2020, soil was frozen only temporarily, the maximum frost depth being less than 10 cm (Fig 4b). The soil frost depth (mean 1 cm) during the winter of 2020 was significantly different compared to the winters of 2016–2022 (mean 9 cm) according to Kruskal-Wallis test $H(1) = 119.19$ ($p<.0001$). This indicates that several freeze-thaw cycles have occurred in the winter of 2020. Based on Fig 4b, the highest turbidity levels occurred simultaneously with low or nonexistent soil frost depths in the winter of 2020.

The winter of 2020 stood out with exceptionally high rain sum and turbidity levels in all of the three stations (Table 5). Based on the monitoring data, the wintertime turbidity variation related to particulate P concentrations in February 2020 seemed to be connected to the precipitation coming as rain. We analysed the differences in turbidity levels between winters and stations by using discharge as a covariate. The analysis of covariance showed that daily turbidities increased more with the discharge during the winter of 2020 than in the other winters in Station 2 ($n = 875$, $p < 0.0001$) as well as in Station 3 ($n = 875$, $p<0.0001$) (Fig 4c). In addition, the correlation between turbidity and discharge was clearly stronger during winter of 2020, compared to winters of 2016–2020. During the winter 2020 the turbidity increase with discharge was more pronounced (had a steeper slope) in Station 3 than in Station 2 whereas usually, the stations had a similar relationship between turbidity and discharge in wintertime.

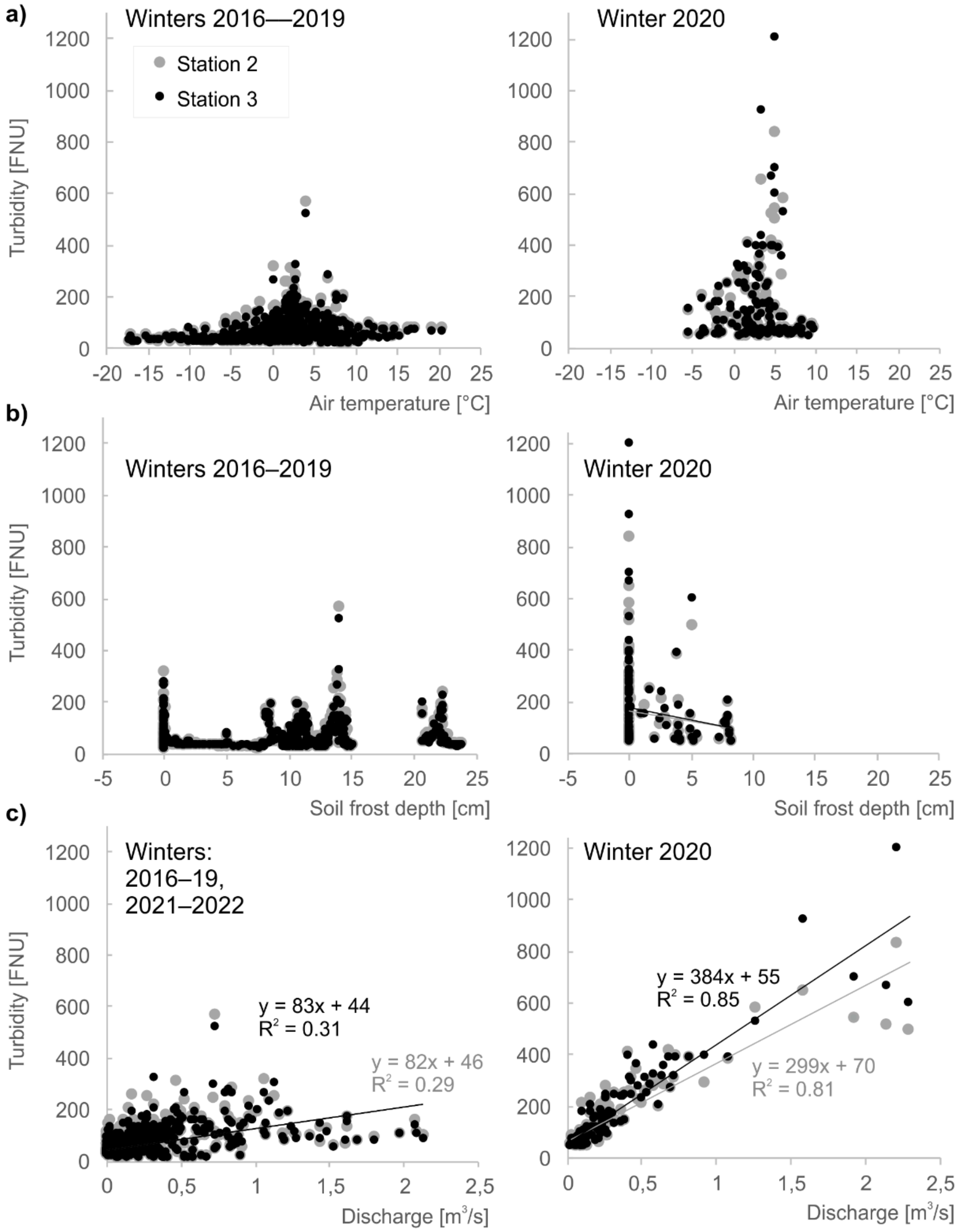

Fig 4. The relationship between daily mean turbidity (FNU, Formazine Nephelometric Units) and the hydro-climatological conditions during winter periods: a) air temperature, b) soil frost depth and c) discharge at the Station 1. during different winter periods.

4.3. Turbidity during high-flow events

The flood event of February 2020 was also compared with other high flow events. During late autumn 2019 and 2020 daily discharges were comparable to February 2020. The highest hourly discharge peaks during each of the events were about 4 m^3/s (Fig. 5, Table 6) and the mean temperatures during each of the observed months were between 0 and 5 degrees. However, the turbidity levels of winter 2020 were notably higher compared to the ones measured during the late autumn high discharges. Furthermore, in February 2020, Station 3 showed higher turbidity peaks compared to Station 2 (Fig 5b). The analysis of covariance confirmed that the hourly measured turbidity of the Station 3 was significantly more increasing with the discharge ($n = 1392$, $p<.0001$) compared to the Station 2 during February 2020 (Fig 5b). Especially the last of the three consecutive high peaks showed a large difference in turbidities between stations 2 and 3. At that time the turbidity increase from Station 2 to Station 3 correlated significantly with discharge (Table 6). During the high autumn flows, by contrast, the turbidity of upper and lower gypsum areas was congruent (Fig 5 a & c) and no such correlations were present.

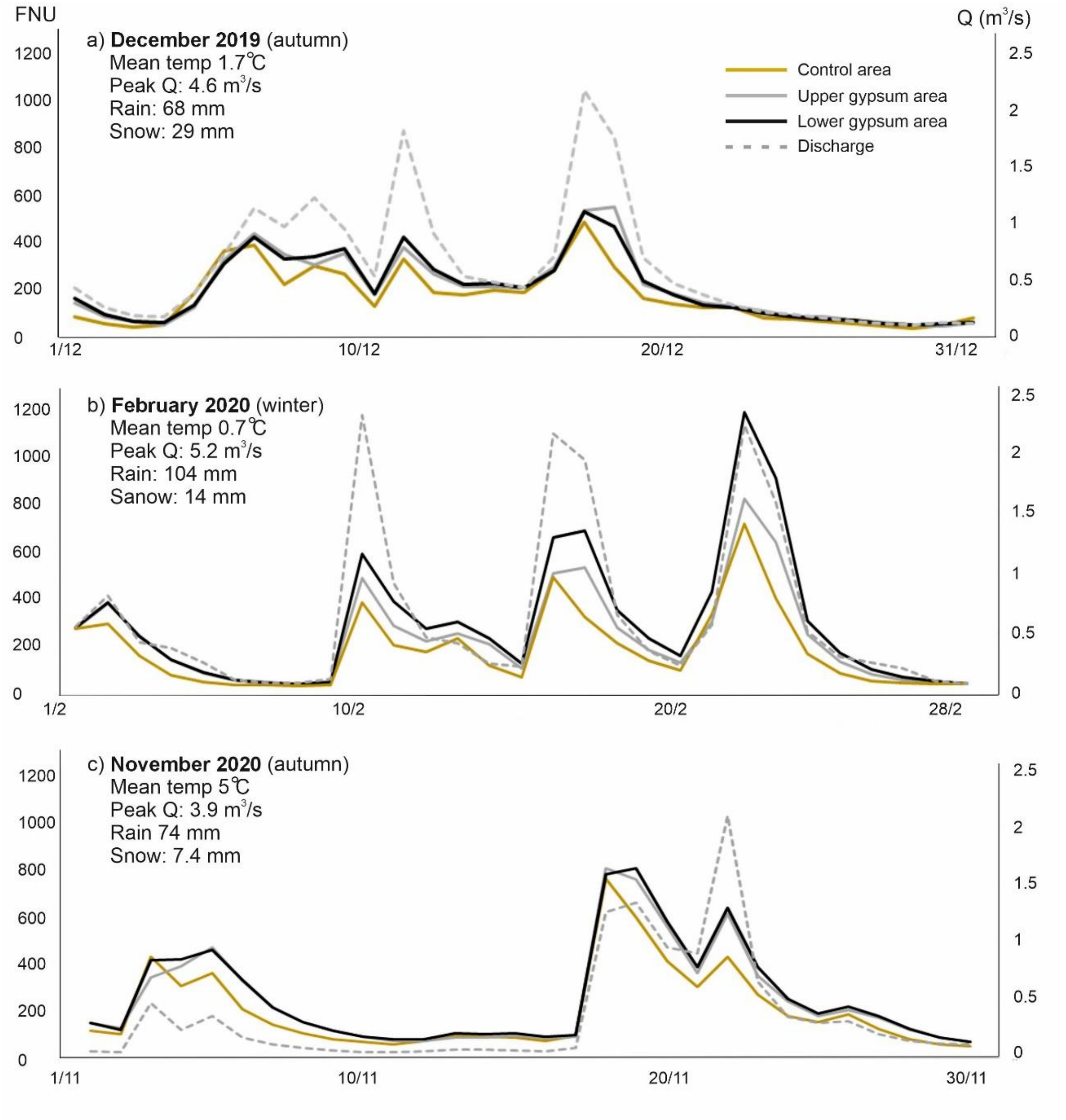

Fig 5. Relationship of discharge and turbidity at points 1,5, and 8 during three high flow events. Time series describe the hourly variation in turbidity in the three riverine monitoring stations during three separate high-flow events. Figs a and c represent autumn periods high flows and b represents February 2020. The discharge values are daily averages of Station 1 and do not show the highest hourly peaks. The monthly mean temperature and peak discharge are marked in the figures.

February 2020 deviated from the two other flood events at least with a higher rain sum and number of preceding FT-cycles (Table 6). Another notable difference between those three high-flow events was the season, and the fact that the vegetation might still prevent erosion on the riverbanks during late autumn. The comparison of the three flow events suggests that the high turbidity peak in February 2020 was a consequence of a combination of several factors, including a prolonged wet period without vegetation, high discharge, high temperatures, low soil frost, and several FT-cycles. However, those do not explain the reason for the extreme increase of turbidity with increased discharge at Station 3. Therefore, in the following chapter, we explore the potential role of erosion power and in-stream erosion processes that may have contributed to this difference in turbidity levels between stations.

Table 6. Statistics of three high-flow events during the study period. Peak turbidity, number of FT-cycles, and the correlation between turbidity and discharge were calculated based on daily averaged values. FT-cycles represents the sum of ground freeze-thaw cycles during the preceding 20 days prior to the turbidity peak. The last column represents the correlation between the increase in turbidity between Stations 2 and 3, and discharge (significant positive correlation on Feb. 2020).

	Peak turbidity (FNU)		**FT-cycles**	**r (FNU vs. Q)**		**r (diff FNU vs. Q)**
	Stat 2	Stat 3	sum	Stat 2	Stat 3	Stat 3- Stat 2
Dec 2019	560	470	4	0.94	0.96	0.14
Feb 2020	840	1200	6	0.92	0.9	**0.81**
Nov 2020	780	780	0	0.86	0.87	0.33

4.4. Erosional power during different flow stages

Three flow events MQ, MHQ, and HQ were simulated in 2D to find out how the inundated areas differed during the flow stages and whether the increased erosion with high flows would explain the turbidity peaks of winter 2020 and especially the exceptionally high turbidity of the lower gypsum area. The inundated areas expanded significantly with the increasing discharge in both areas (Table 7). With the discharge increasing from MHQ to HQ, the inundated area more than doubled in the lower gypsum area, while in the upper area, the increase was 65 %.

The flow velocity initiating the motion of clay particles (~1 m/s) was used as a threshold value to determine potential erosion areas (later “erosional area”) in order to compare how likely and from what extent the particles could be resuspended by different flow rates (Hjulström, 1935). Based on the modelling results, the percentage increase in erosional area (flow velocity > 1 m/s) was much larger in the lower than the upper gypsum area (Table 7). The most notable increase was related to the discharge increase from medium discharge (MQ) to medium flood (MHQ), between which the proportion of the erosional area increased by more than 700% in the lower gypsum area. However, also the increase of erosion from MHQ to HQ was larger in the lower gypsum area: the erosional areas increased by 106 % and 60% in the lower and upper areas, respectively. The areas with the most significant increase in erosion between discharges were rather evenly distributed along the river reaches (Figs 6 & 7). However, two erosional zones were identified from both modelling domains (Zones 1-4) to get more insights into the characteristic of those areas.

Table 7. *The total inundated area and erosional area (in ha) where velocities exceed the initiation of motion of clay particles (1 m/s) based on modeling results of different flow scenarios at the upper and lower gypsum areas. The proportion of the erosional area from*

the total inundated area is in the parentheses. The increase of erosional area (in %) between the flow scenarios

	Upper gypsum area (ha)	Lower gypsum area (ha)
MQ		
Total inundated area	6.44	2.88
Erosional area	0.24 (3,7 %)	0.08 (2.8 %)
MHQ		
Total inundated area	11.91	5.16
Erosional area	0.81 (68%)	0.66 (12.8 %)
HQ		
Total inundated area	19.7	12,13
Erosional area	1.3 (6.6 %)	1.36 (11.2 %)
Increase of erosional area		
MQ to MHQ	237%	725%
MQ to HQ	442%	1600%
MHQ to HQ	60%	106%

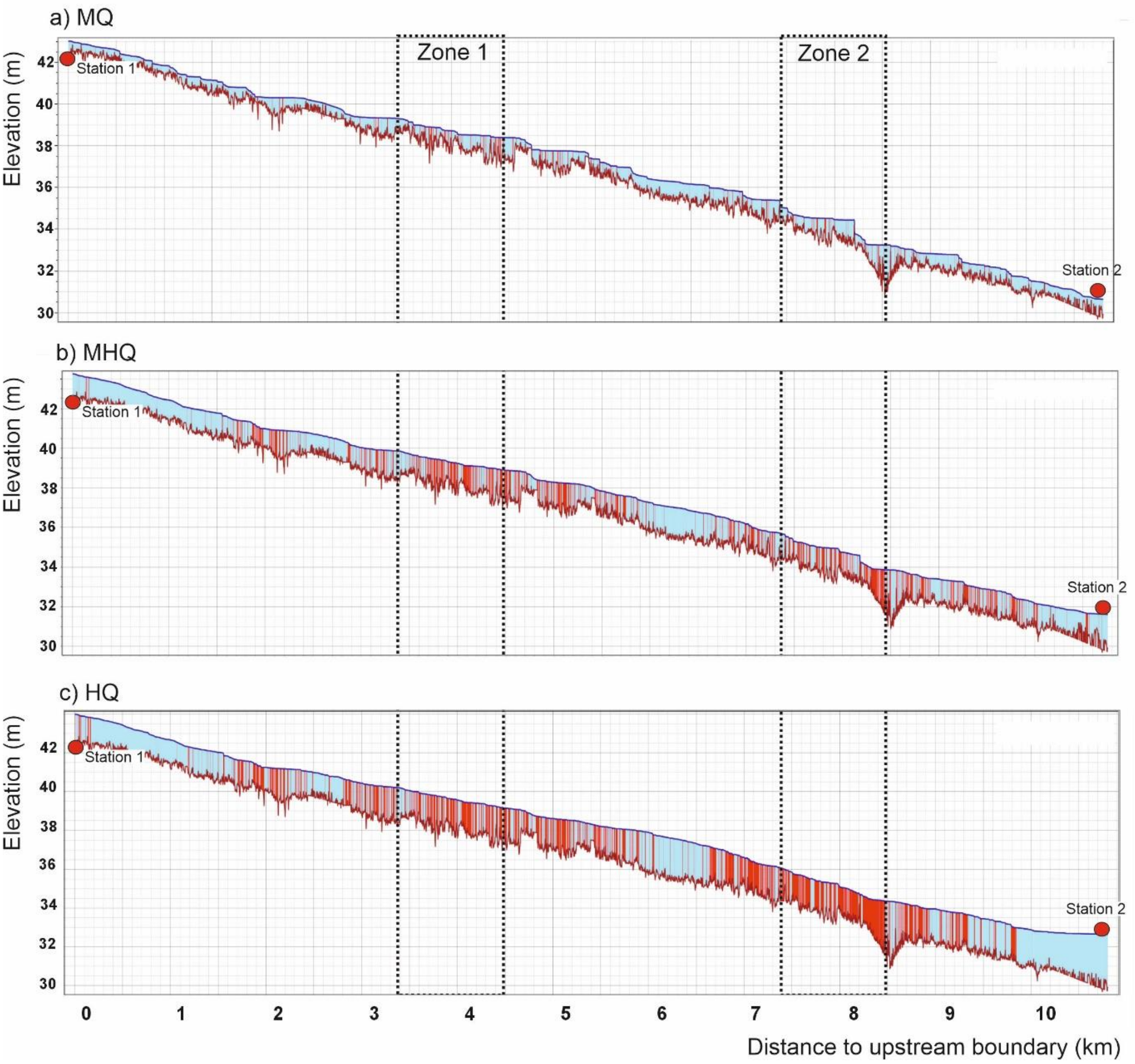

Fig 6. Longitudinal profile of the upper gypsum area with modelled flow depth and erosional areas during a) MQ b) MHQ and c) HQ. The blue areas describe flow depth while the erosional areas of clay are marked with red colour. Two erosional zones (Zones 1 and 2) were identified. In these zones, the channel area where clay is potentially eroded increased significantly as the flow rate increased. The monitoring Stations 1 and 2, at the upstream and downstream boundariesare marked in the figure.

At the upper gypsum area both Zones 1 and 2 were meandering and the river reach was partly lacking a vegetated buffer zone (Figs. 8 & 9). However, especially in Zone 1, the inundated area hardly reached the fields even during the high flow (Fig. 8c). On that reach the erosional areas increased in the channel thalweg in both curved and straight reaches. By contrast, the flood waters reached the fields extensively in Zone 2 during high discharge (HQ), even though the actual erosional areas were quite evenly distributed along the stream, and no erosional areas were outside of the main channel (Fig.9c).

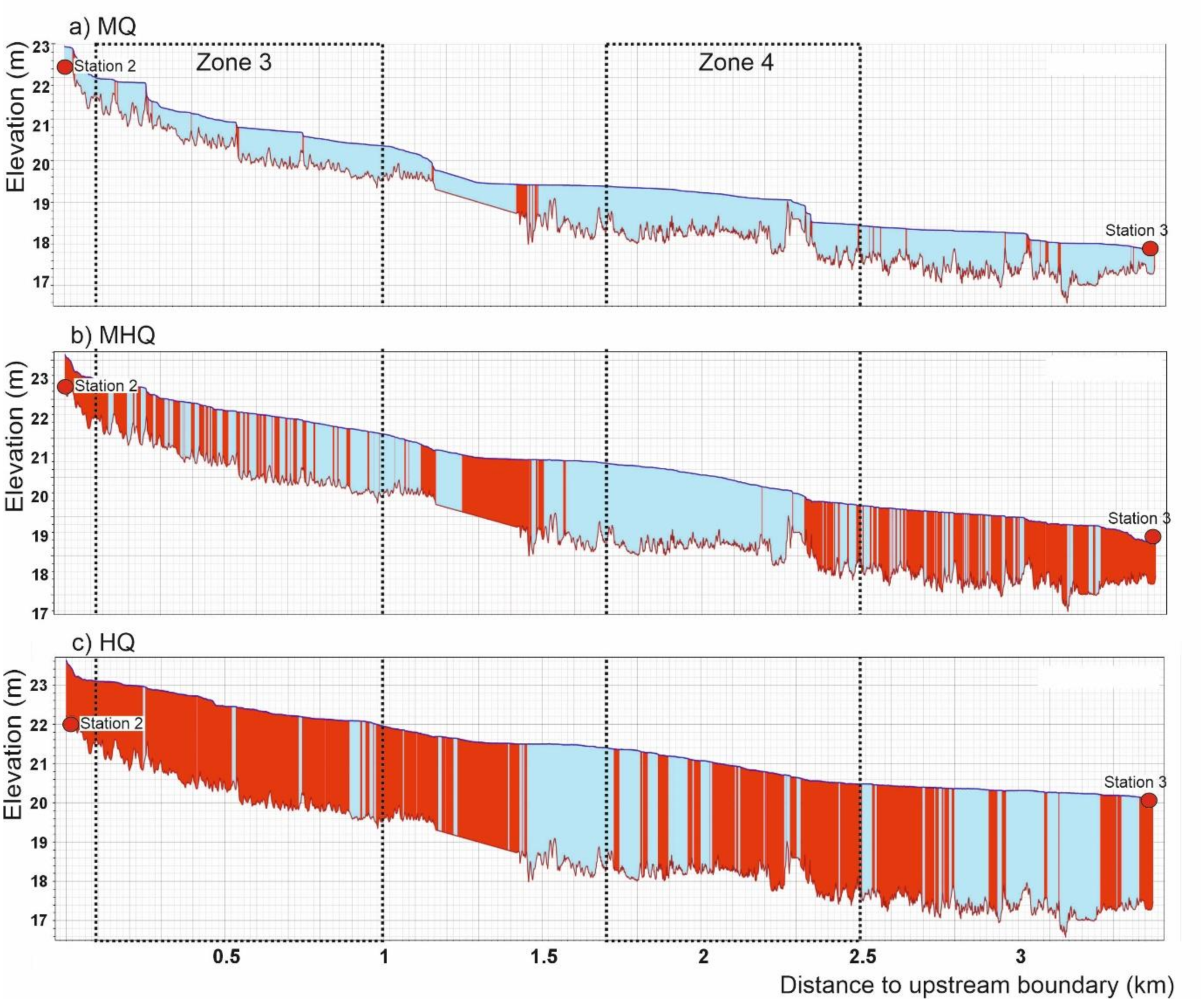

Fig 7. Longitudinal profile of the lower gypsum area with modelled flow depth and erosional areas during a) HQ b) MHQ and c) MQ. The blue areas describe flow depth while the

erosional areas of clay are marked with red colour. Two erosional zones (Zones 3 and 4) were identified. In these zones, the channel area where clay is potentially eroded increased significantly as the flow rate increased. The water quality monitoring station (Station 3) is located at the outlet of the lower gypsum area.

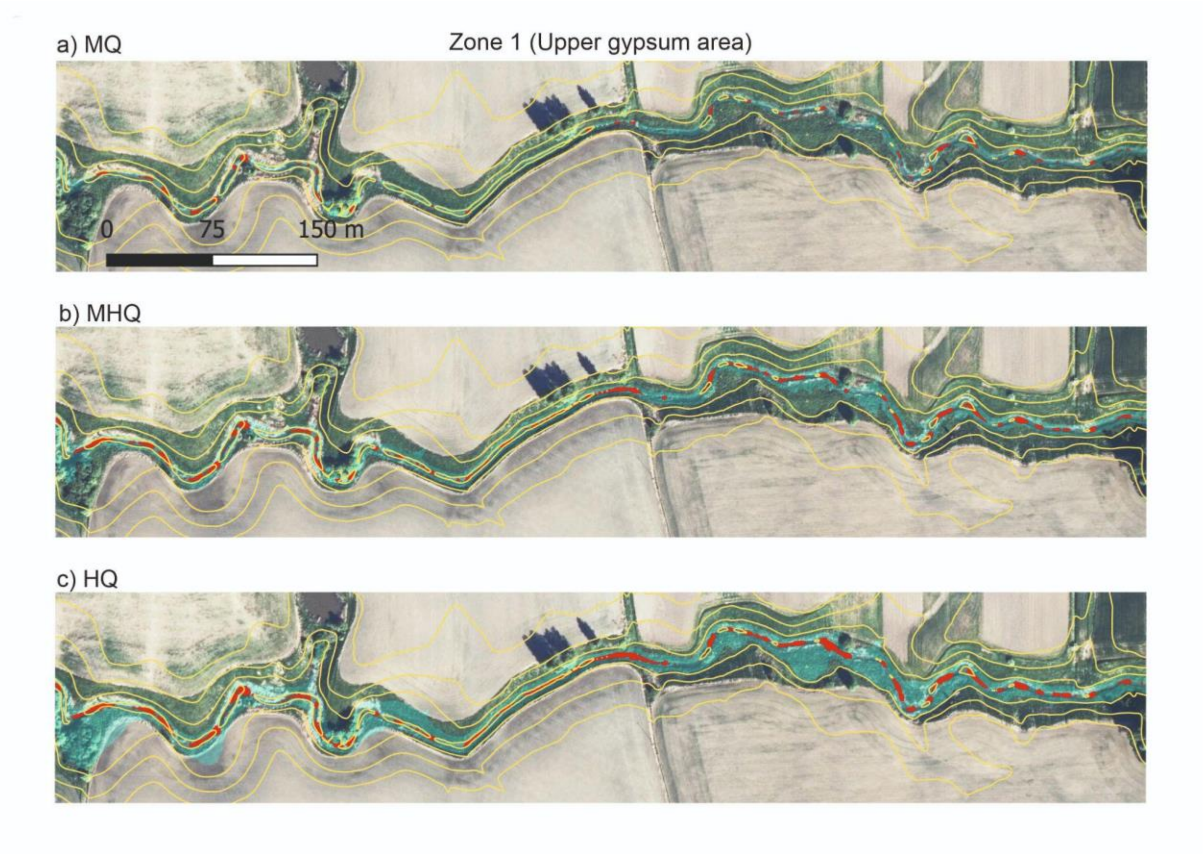

Fig. 8. Erosional Zone 1. The zone is extracted from the upper gypsum area (see Fig. 6). The contour interval is 2 m. The erosional areas of clay (flow velocity > 1m/s) are marked with red and the inundated area with transparent blue.

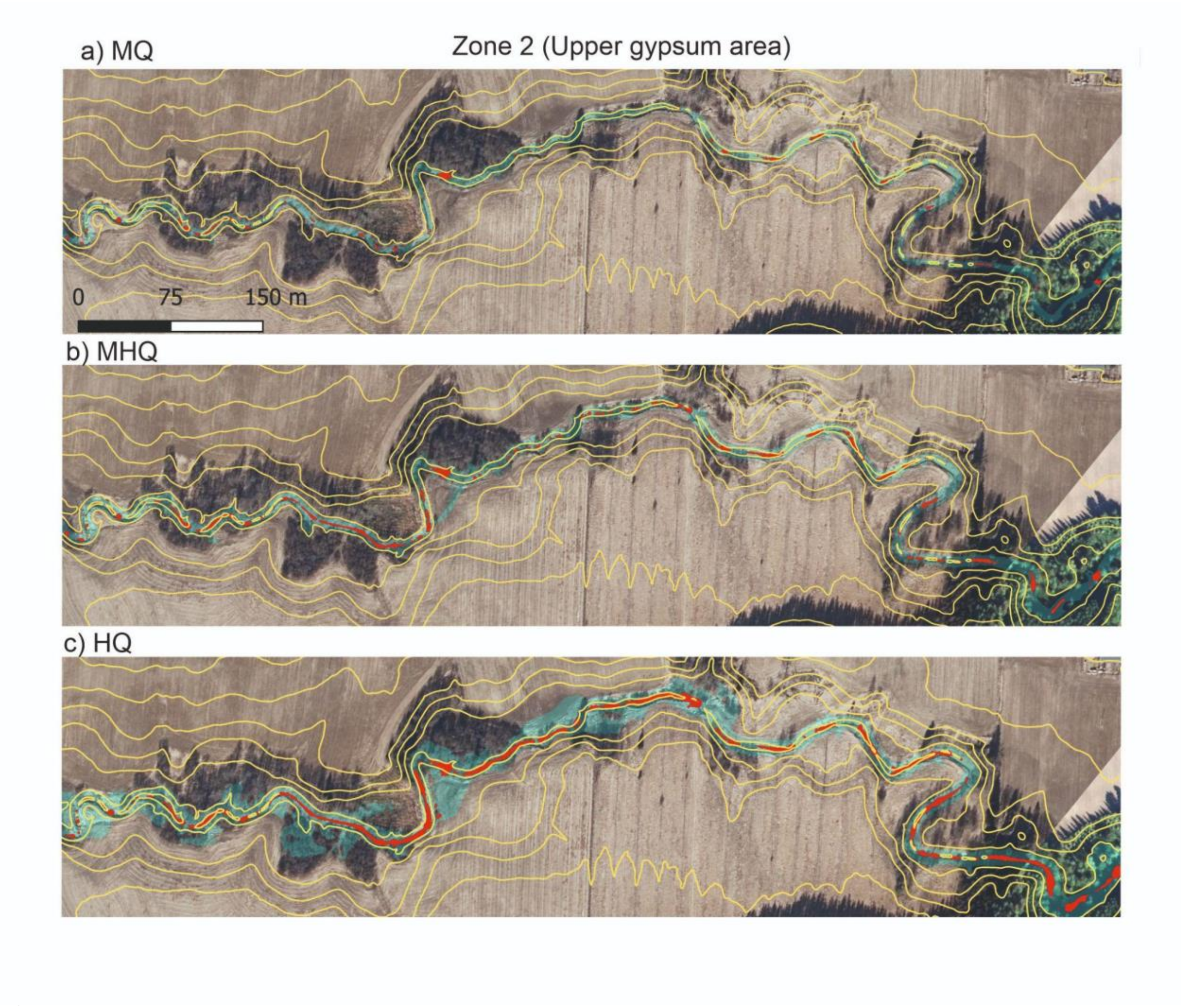

Fig. 9. Erosional Zone 2. The zone is extracted from the upper gypsum area (see Fig. 6). The contour interval is 2m. The erosional areas of clay (flow velocity > 1m/s) are marked with red and the inundated area with transparent blue.

Based on the hydraulic model, only 2,8 % of the inundated area had flow velocities capable of eroding clay during the mean flow (Table 7). Especially in the selected zones (Zones 3 & 4) in the lower area, the erosion was negligible at the mean discharge (Figs. 10a & 11a). Even with a medium flood (MHQ) the erosional areas were only a few, especially in Zone 4 (Fig 7). In Zone 3, velocities capable of eroding clay were modelled for almost the entire reach at high discharge (Fig. 10c). The flood extended slightly onto the fields even during the MHQ situation on both Zones 3 and 4. During the HQ event, the water overflowed outside the channel, spread onto the fields and abandoned channels, and adopted new pathways in Zone 3 (Fig. 10c). The erosional areas with flow velocities > 1 m/s were modeled even over the flood plains, adding notably the potential of the aggregated matter originated from gypsum amendment to resuspend. In Zone 4 the flooding over the fields was notable during HQ, but the erosional areas were mainly located in the main channel (Fig. 11c).

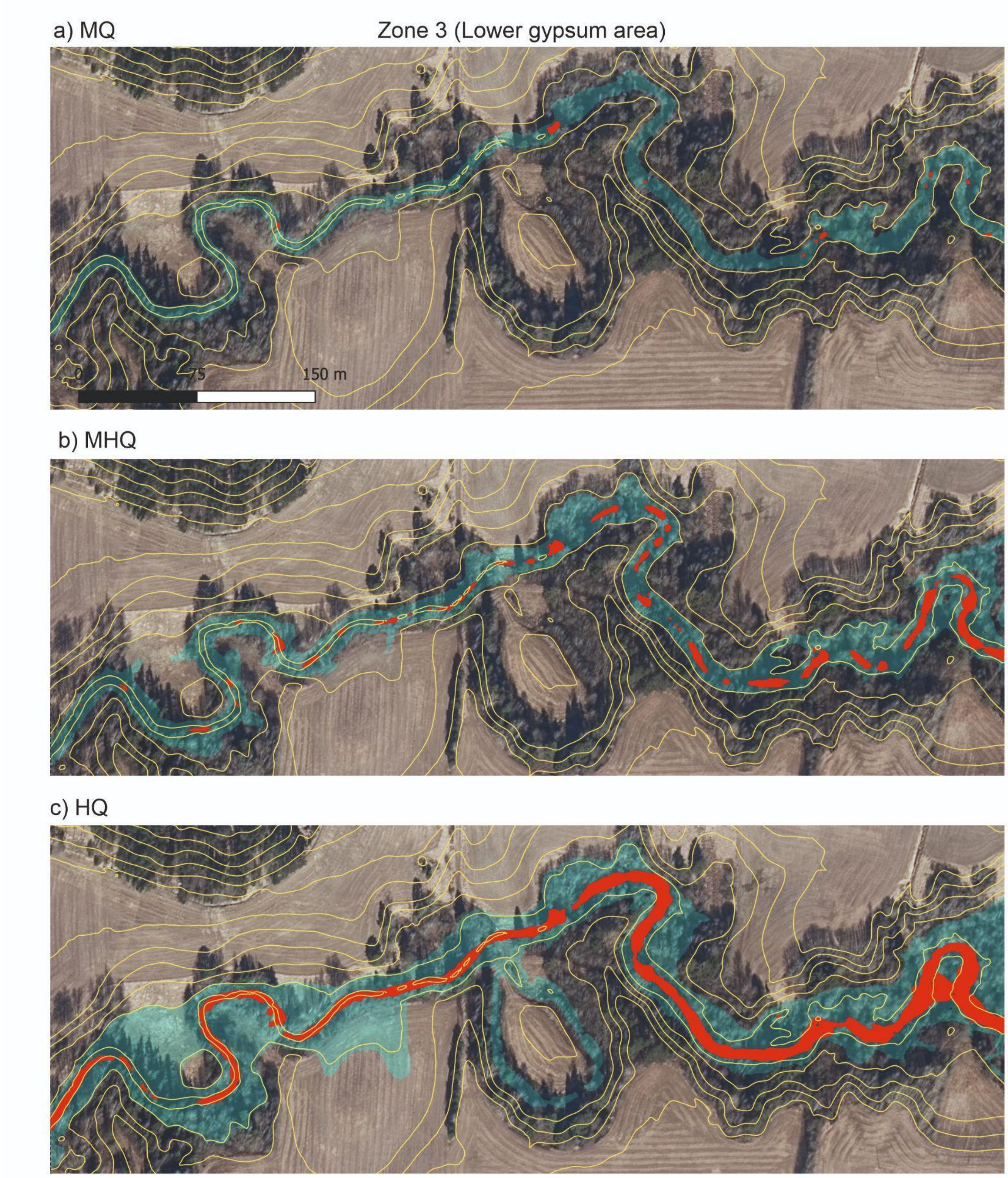

Fig. 10. Erosional Zone 3. The zone is extracted from the lower gypsum area (see Fig. 7). The contour interval is 2 m. The erosional areas of clay (flow velocity > 1 m/s) are marked with red and the inundated area with transparent blue.

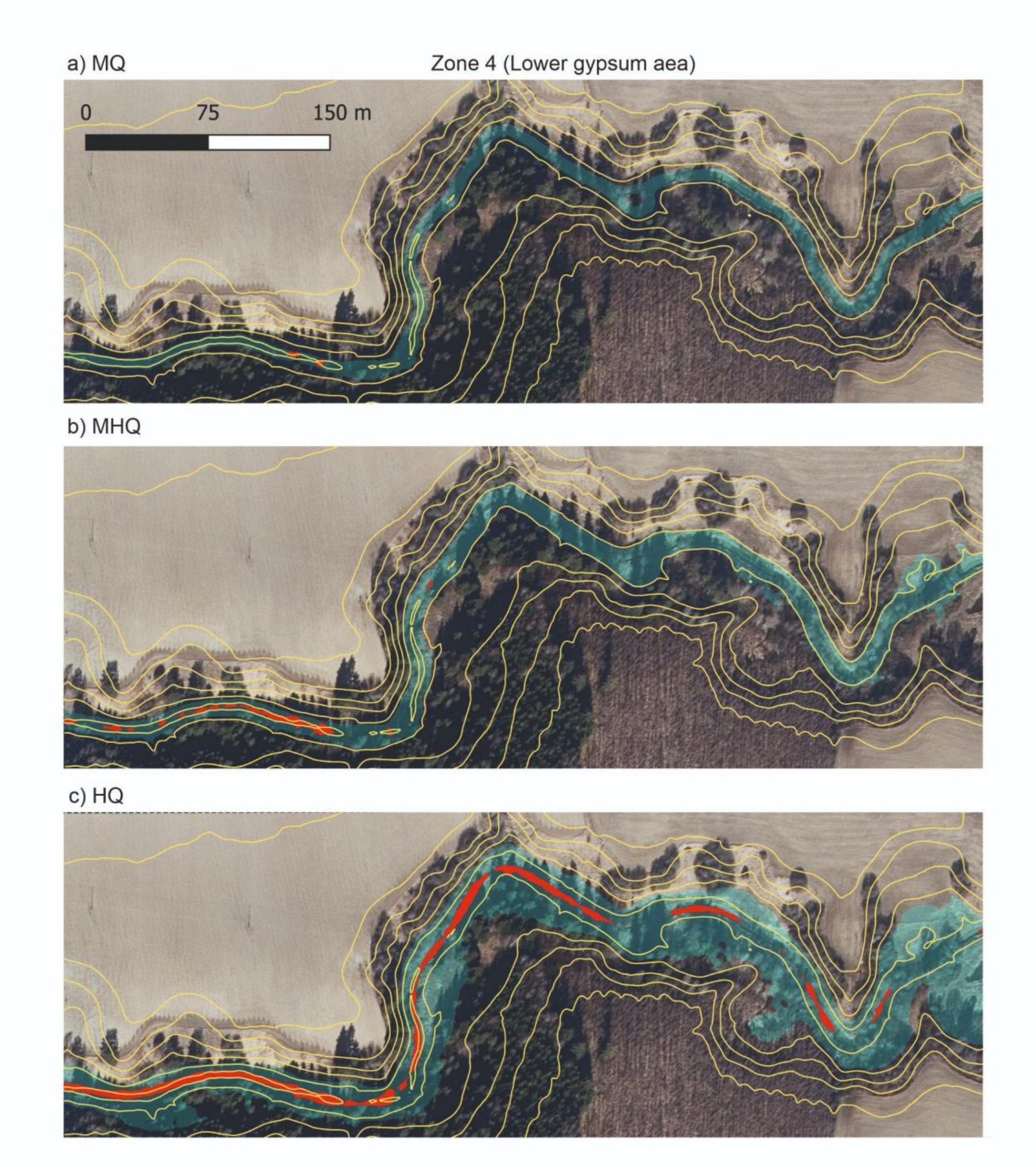

Fig. 11. Erosional Zone 4. The zone is extracted from the lower gypsum area (see fig. 7). The contour interval is 2 m. The erosional areas of clay (flow velocity > 1 m/s) are marked with red and the inundated area with transparent blue.

5. Discussion

Demonstrating the effect of measures targeting nutrient loads with watershed-scale measurements is challenging, as the impact may be obscured e.g. by hydrological variations and in-stream processes (Puustinen et al., 2007, Withers and Jarvie, 2008). In fact, despite the increased usage of gypsum in combating eutrophication by preventing phosphorus loads (King et al., 2016; Kost et al., 2018; Mao et al., 2023), not much is known about the functionality and efficiency of gypsum treatment as a large-scale measure in different environmental and climatological conditions. This is partly due to only few catchment-scale studies on gypsum efficiency (Cox et al., 2005; Varcoe et al., 2010; Ekholm et al., 2024).

Our focus on winter conditions stems from the anticipated rise in warming and precipitation in the northern Baltic Sea region during this season, potentially intensifying erosion and phosphorus losses (Huttunen et al., 2015). Our monitoring data revealed a clear correlation between discharge and turbidity especially during winter and autumn, which was even emphasized during a warm winter. The turbidity levels during the extremely wet and warm winter of 2020 were twice as high as in the other winter periods with snow-melt-induced peak discharges. The precipitation coming as rain, clearly increased the winter time turbidity. Summer rains did not increase turbidity notably, which is explained by the vegetation cover preventing erosion and high evapotranspiration inhibiting very high discharges. Even though the turbidity levels are usually highest during autumns, the winter 2020 showed even higher turbidities, when comparing the data from February 2020 with other high flow events occurring outside of the winter period. These observations support many previous works indicating that the catchment-originated sediment yields may increase in boreal areas with increasing wet future winters, as the erosion is enhanced by the absence of vegetation making the soil more prone to erosion (Inamdar et al., 2018; Puustinen et al., 2007; Salmela et al., 2022).

Typically in the seasonally frozen environments, the bulk of the erosion and particulate P loading from agricultural lands is concentrated outside the growing season driven by high discharges like spring snowmelt, soil P status, and the lack of a protective vegetation layer (Bennett et al., 2001; Casson et al., 2019; Puustinen et al., 2007). In those areas, the soil frost may hinder the erosion and therefore instantaneous P loss, while the FT-cycles occurring during the winter have been stated to have the opposite effect (Sun et al., 2021). FT-cycle destroys soil structure and enhances P release and its transport along with runoff, soil water and heat movement (Zhao et al., 2021). A laboratory test by Ferric & Gatto (2005) indicated that especially the co-effect of soil moisture and FT-cycles may increase soil erosion dramatically. During the wet February 2020, several FT cycles occurred supporting the finding of Ferrick and Gatto, (2005): more than 10 topsoil freezes and thaws were experienced prior to the turbidity peak (Fig. 13 in supplementary material). This distinguishes February 2020 from two other monitored high-flow events, occurring in the late autumns of 2019 and 2020, with notably lower turbidity. The long FT-cycle period preceding the turbidity peak in February 2020 has likely contributed to the turbidity increase. Our results and literature indicate that the FT-cycles and soil frost dynamics should be carefully considered when interpreting the monitoring results and assessing the effectiveness of gypsum treatment. If warm and wet winters continue to increase in the hemiboreal climate zone in the future, the FT-cycles are predicted to become more frequent, subsequently increasing overall erosion. Further research is needed to understand how the increasing FT-cycles may impact the effectiveness of gypsum treatment in preventing phosphorus losses. This requires studies examining the connection between FT cycles, erosion, and its spatial distribution.

However, neither the FT-cycle nor the high discharge or seasonality explain the observed significantly higher concentrations in the lower gypsum area in February 2020, compared to the upper gypsum area. Stream erosion and the resuspension of settled particles could explain this difference: the flow velocities eroding clay were modelled along the entire reach during the high flow, suggesting high connectivity of the system (Wohl, 2017). The high connectivity enables suspended sediment transport throughout the system potentially adding to the turbidity towards the catchment outlet, which may explain the emphasized increase in turbidity at the downstream measurement station during very high flows. In addition, based on the hydraulic modeling of three different flow stages, both the inundated and clay-erodible areas in the lower gypsum area expanded proportionally much more during a major flood: based on the modelling results, the area in which flow velocities eroding clay were exceeded expanded up to 16-fold during the high-flow situation (HQ) compared to average flow (MQ) in the lower gypsum area. The corresponding increase in the upper area was 4.4-fold. The inundated area also expanded proportionally much more in the lower area than in the upper area with increasing discharge. For example, as the flow increased from average flood (MHQ) to high flood (HQ), the inundated area more than doubled in the lower gypsum area, while in the upper area, the increase was only 65%.

Furthermore, in the lower area, flow velocities eroding clay were modelled even on fields and barren areas during high flow, notably adding to the potential of resuspension from gypsum-originated aggregated matter. These results suggest that during an extremely high flow in February 2020, more erosion occurred both in the channel and outside the channel in the lower gypsum area compared to the upper area leading to higher turbidity values. This assumption is supported by the study of Gellis and Noe (2013), stating that stream bank erosion can contribute with a similar magnitude as agricultural land to the annual fine-grained suspended sediment load. It is also generally known that the runoff concentrations of particulate phosphorus remain significantly lower in fields with permanent crop cover during wet and warm winters (Puustinen et al., 2007). This study supports this claim and suggests that as high winter flows increase, it is crucial to consider permanent vegetation on fields for their water-protective effect.

Modeling provided spatially comprehensive information about the monitoring area and allowed investigating major flood situation in the absence of measurement data. However, it should be noted that the performance of modelling depends on the available input data and that modelling is always an estimation. In this study, the boundary conditions of the major flood were based on estimates derived by extrapolating from other measurements, as not enough data was available from the flood event. In addition, the model calibration was performed using the upper gypsum area only, due to data availability. Therefore, caution should be used when interpreting modeling results, considering them at best indicative, and focusing on examining relative differences between the areas and flood events, rather than absolute values.

6. Conclusions

The results of this catchment scale study suggest that the performance of gypsum could be dependent on seasonal and climatological variations. Based on the analysis of 5 years monitoring data of water quality, quantity, and climate variables on a boreal catchment, it seems that the season, weather, and flow stage all affect the nutrient loads from gypsum-treated agricultural fields.

As the gypsum treatment operating principle is directly linked to preventing erosion, the combined effect of lack of vegetation and soil frost during winters is causing the most challenging circumstances for gypsum. Even though the winter time turbidities usually remain low, the frequent FT-cycles, high discharges, and precipitation coming as rain may induce high wintertime turbidities. Precipitation coming as rain increases turbidity even more during winter time compared to other seasons. The winter conditions challenging the gypsum efficacy i.e. rain-induced high flows together with loose material of the wetted soil, intensified by the FT-cycle and the lack of binding vegetation, are going to become more frequent in the future in the boreal climate area. It is thus crucial to consider wintertime vegetation on the fields for its water-protective effect, keeping in mind their potential adverse effect on dissolved P. Summer rains and high discharges do not affect turbidity levels notably.

It also seems likely that the erosion and resuspension of the material from the stream bed, intensified with high connectivity of the river system, may have an impact on turbidity and thus on phosphorus emissions downstream. When comparing the gypsum response differences experienced in two gypsum amendment areas, our hydraulic modeling results revealed that major flood situations expanded the inundated area and increased stream erosion notably more in the area which also experienced much higher turbidity values during the flood situation in focus. This suggests that particles settled on the riverbed during low discharges could resuspend during high discharge events, reducing the long-term effect of gypsum amendment and making the gypsum's performance dependent on discharge variations and stream morphology.

This unique study setting confirmed that catchment-scale study with a spatially comprehensive monitoring, considering both water quality and hydro-climatological phenomena, is needed to be able to reliably study the functionality of different nutrient load reduction actions, including gypsum amendment.

References

Appelo, C.A.J., Postma, D., 2005. Geochemistry, Groundwater and Pollution, 2nd ed. CRC Press, London. https://doi.org/10.1201/9781439833544

Arheimer, B., Dahné, J., Donnelly, C., 2012. Climate Change Impact on Riverine Nutrient Load and Land-Based Remedial Measures of the Baltic Sea Action Plan. AMBIO 41, 600–612. https://doi.org/10.1007/s13280-012-0323-0

Aura, E., Saarela, K., Räty, M., 2006. Savimaiden eroosio.

Barnes, H.H., 1967. Roughness characteristics of natural channels (No. 1849), Water Supply Paper. U.S. Govt. Print. Off.,. https://doi.org/10.3133/wsp1849

Bennett, E.M., Carpenter, S.R., Caraco, N.F., 2001. Human Impact on Erodable Phosphorus and Eutrophication: A Global Perspective: Increasing accumulation of phosphorus in soil threatens rivers, lakes, and coastal oceans with eutrophication. BioScience 51, 227–234. https://doi.org/10.1641/0006-3568(2001)051[0227:HIOEPA]2.0.CO;2

Casson, N.J., Wilson, H.F., Higgins, S.M., 2019. Hydrological and Seasonal Controls of Phosphorus in Northern Great Plains Agricultural Streams. J. Environ. Qual. 48, 978–987. https://doi.org/10.2134/jeq2018.07.0281

Cox, J.W., Varcoe, J., Chittleborough, D.J., van Leeuwen, J., 2005. Using gypsum to reduce phosphorus in runoff from subcatchments in South Australia. J. Environ. Qual. 34, 2118–2128. https://doi.org/10.2134/jeq2005.0013

Ekholm, P., Ollikainen, M., Punttila, E., Ala-Harja, V., Riihimäki, J., Kiirikki, M., Taskinen, A., Begum, K., 2024. Gypsum amendment of agricultural fields to decrease phosphorus losses – Evidence on a catchment scale. J. Environ. Manage. 357, 120706. https://doi.org/10.1016/j.jenvman.2024.120706

Ekholm, P., Valkama, P., Jaakkola, E., Kiirikki, M., Lahti, K., Pietola, L., 2012. Gypsum amendment of soils reduces phosphorus losses in an agricultural catchment. Agric. Food Sci. 21, 279–291. https://doi.org/10.23986/afsci.6831

Ferrick, M.G., Gatto, L.W., 2005. Quantifying the effect of a freeze–thaw cycle on soil erosion: laboratory experiments. Earth Surf. Process. Landf. 30, 1305–1326. https://doi.org/10.1002/esp.1209

ELY, 2024. KIPSI-hanke. [WWW Document]. https://www.ely-keskus.fi/web/kipsinlevitys/hanke-esittely (accessed 4.16.24).

FMI, 2022. Ilmaso-opas [WWW Document]. URL . https://www.ilmasto-opas.fi/artikkelit/varsinais-suomi-tyypillista-tammivyohykkeen-ilmastoa (accessed 1.16.24).

Gellis, A.C., Noe, G.B., 2013. Sediment source analysis in the Linganore Creek watershed, Maryland, USA, using the sediment fingerprinting approach: 2008 to 2010. J. Soils Sediments 13, 1735–1753. https://doi.org/10.1007/s11368-013-0771-6

Higgins, B.P.J., Mohleji, S.C., Irvine, R.L., 1976. Lake Treatment with Fly Ash, Lime, and Gypsum. J. Water Pollut. Control Fed. 48, 2153–2164.

Hjulström, F., 1935. Studies of the morphological activity of rivers as illustrated by the River Fyris. Inaugural dissertation,. Almqvist & Wiksells, Uppsala.

Huttunen, I., Huttunen, M., Piirainen, V., Korppoo, M., Lepistö, A., Räike, A., Tattari, S., Vehviläinen, B., 2016. A National-Scale Nutrient Loading Model for Finnish Watersheds—VEMALA. Environ. Model. Assess. 21, 83–109. https://doi.org/10.1007/s10666-015-9470-6

Huttunen, I., Hyytiäinen, K., Huttunen, M., Sihvonen, M., Veijalainen, N., Korppoo, M., Heiskanen, A.-S., 2021. Agricultural nutrient loading under alternative climate, societal and manure recycling scenarios. Sci. Total Environ. 783, 146871. https://doi.org/10.1016/j.scitotenv.2021.146871

Hydrologic Engineering Center, 2023. HEC-RAS.

Inamdar, S., Johnson, E., Rowland, R., Warner, D., Walter, R., Merritts, D., 2018. Freeze–thaw processes and intense rainfall: the one-two punch for high sediment and nutrient loads from mid-Atlantic watersheds. Biogeochemistry 141, 333–349. https://doi.org/10.1007/s10533-017-0417-7

Kämäri, M., Tarvainen, M., Kotamäki, N., Tattari, S., 2020. High-frequency measured turbidity as a surrogate for phosphorus in boreal zone rivers: appropriate options and critical situations. Environ. Monit. Assess. 192, 366. https://doi.org/10.1007/s10661-020-08335-w

King, K.W., Williams, M.R., Dick, W.A., LaBarge, G.A., 2016. Decreasing Phosphorus Loss in Tile-Drained Landscapes Using Flue Gas Desulfurization Gypsum. J. Environ. Qual. 45, 1722–1730. https://doi.org/10.2134/jeq2016.04.0132

Kost, D., Nester, J., Dick, W.A., 2018. Gypsum as a soil amendment to enhance water quality by reducing soluble phosphorus concentrations. J. Soil Water Conserv. 73, 22A-24A. https://doi.org/10.2489/jswc.73.1.22A

Lilja, H., Uusitalo, R., Yli-Halla, M., Nevalainen, R., Väänänen, T., Tamminen, P., 2009. Suomen maannostietokanta. Käyttöopas versio 1.0.

Mao, Y., Li, X., Dick, W.A., Cao, L., 2023. Use of flue gas desulfurization gypsum to reduce dissolved phosphorus in runoff and leachate from two agricultural soils. Soil Ecol. Lett. 5, 128–136. https://doi.org/10.1007/s42832-022-0135-5

Ollikainen, M., Kosenius, A.-K., Punttila, E., Ala-Harja, V., Puroila, S., Iho, A., Ekholm, P., 2020. Gypsum amendment of arable fields as a water protection measure – farmers’ experience, phosphorus reduction potential and associated costs drawn from a large scale pilot. Agric. Food Sci. 29, 383–394. https://doi.org/10.23986/afsci.88902

Paerl, H.W., Paul, V.J., 2012. Climate change: Links to global expansion of harmful cyanobacteria. Water Res., Cyanobacteria: Impacts of climate change on occurrence, toxicity and water quality management 46, 1349–1363. https://doi.org/10.1016/j.watres.2011.08.002

Pavlidou, A., Giani, M., Yakushev, E.V., 2024. Editorial: Interaction between climate change and anthropogenic pressures in the eutrophication process - volume II. Front. Mar. Sci. 11. https://doi.org/10.3389/fmars.2024.1399298

Pietiläinen, O.-P., Ekholm, P., 1992. Origin of eroded material in a small agricultural drainage basin in southwestern Finland. Aqua Fenn. 22, 105–110.

Puustinen, M., Tattari, S., Koskiaho, J., Linjama, J., 2007. Influence of seasonal and annual hydrological variations on erosion and phosphorus transport from arable areas in Finland. Soil Tillage Res. 93, 44–55. https://doi.org/10.1016/j.still.2006.03.011

Räike, A., Taskinen, A., Knuuttila, S., 2020. Nutrient export from Finnish rivers into the Baltic Sea has not decreased despite water protection measures. Ambio 49, 460–474. https://doi.org/10.1007/s13280-019-01217-7

Rankinen, K., Keinänen, H., Cano Bernal, J.E., 2016. Influence of climate and land use changes on nutrient fluxes from Finnish rivers to the Baltic Sea. Agric. Ecosyst. Environ. 216, 100–115. https://doi.org/10.1016/j.agee.2015.09.010

Salmela, J., Saarni, S., Blåfield, L., Katainen, M., Kasvi, E., Alho, P., 2022. Comparison of cold season sedimentation dynamics in the non-tidal estuary of the Northern Baltic Sea. Mar. Geol. 443, 106701. https://doi.org/10.1016/j.margeo.2021.106701

Shainberg, I., Sumner, M.E., Miller, W.P., Farina, M.P.W., Pavan, M.A., Fey, M.V., 1989. Use of Gypsum on Soils: A Review, in: Stewart, B.A. (Ed.), Advances in Soil

Science: Volume 9. Springer US, New York, NY, pp. 1–111. https://doi.org/10.1007/978-1-4612-3532-3_1

Skarbøvik, E., Gyritia Madsen van't Veen, S., Lannergård, E.E., Wenng, H., Stutter, M., Bieroza, M., Atcheson, K., Jordan, P., Fölster, J., Mellander, P.-E., Kronvang, B., Marttila, H., Kaste, Ø., Lepistö, A., Kämäri, M., 2023. Comparing in situ turbidity sensor measurements as a proxy for suspended sediments in North-Western European streams. CATENA 225, 107006. https://doi.org/10.1016/j.catena.2023.107006

Sun, B., Ren, F., Ding, W., Zhang, G., Huang, J., Li, J., Zhang, L., 2021. Effects of freeze-thaw on soil properties and water erosion. Soil Water Res. 16, 205–216. https://doi.org/10.17221/143/2020-SWR

SYKE, 2022. Vesikartta. [WWW Document]. https://paikkatieto.ymparisto.fi/vesikarttaviewers/Html5Viewer_4_14_2/Index.html?configBase=https://paikkatieto.ymparisto.fi/Geocortex/Essentials/REST/sites/VesikarttaKansa/viewers/VesikarttaHTML525/virtualdirectory/Resources/Config/Default&locale=fi-FI (accessed 4.16.24).

Tilman, D., Fargione, J., Wolff, B., D'Antonio, C., Dobson, A., Howarth, R., Schindler, D., Schlesinger, W.H., Simberloff, D., Swackhamer, D., 2001. Forecasting Agriculturally Driven Global Environmental Change. Science 292, 281–284. https://doi.org/10.1126/science.1057544

Uusitalo, R., Ylivainio, K., Hyväluoma, J., Rasa, K., Kaseva, J., Nylund, P., Pietola, L., Turtola, E., 2012. The effects of gypsum on the transfer of phosphorus and other nutrients through clay soil monoliths. Agric. Food Sci. 21, 260–278. https://doi.org/10.23986/afsci.4855

Varcoe, J., Leeuwen, J.A. van, Chittleborough, D.J., Cox, J.W., Smernik, R.J., Heitz, A., 2010. Changes in water quality following gypsum application to catchment soils of the Mount Lofty Ranges, South Australia. Org. Geochem., 2008 Australian Organic Geochemistry Conference: A national conference held in association with the International Humic Substances Society and the Natural Organic Matter Interest Group 41, 116–123. https://doi.org/10.1016/j.orggeochem.2009.09.010

Vehviläinen, B., Huttunen, M., 2001. Hydrological Forecasting and Real Time Monitoring in Finland : The Watershed Simulation and Forecasting System (WSFS).

Verduin, 1969. Man’s Influence on Lake Erie. Ohi0 J. Sci. 69, 65–70.

Vigouroux, G., Destouni, G., 2022. Gap identification in coastal eutrophication research – Scoping review for the Baltic system case. Sci. Total Environ. 839, 156240. https://doi.org/10.1016/j.scitotenv.2022.156240

Vitousek, P.M., Naylor, R., Crews, T., David, M.B., Drinkwater, L.E., Holland, E., Johnes, P.J., Katzenberger, J., Martinelli, L.A., Matson, P.A., Nziguheba, G., Ojima, D., Palm, C.A., Robertson, G.P., Sanchez, P.A., Townsend, A.R., Zhang, F.S., 2009. Nutrient Imbalances in Agricultural Development. Science 324, 1519–1520. https://doi.org/10.1126/science.1170261

Wang, M., Kroeze, C., Strokal, M., van Vliet, M.T.H., Ma, L., 2020. Global Change Can Make Coastal Eutrophication Control in China More Difficult. Earths Future 8, e2019EF001280. https://doi.org/10.1029/2019EF001280

Zhao, Y., Li, Y., Yang, F., 2021. Critical review on soil phosphorus migration and transformation under freezing-thawing cycles and typical regulatory measurements. Sci. Total Environ. 751, 141614. https://doi.org/10.1016/j.scitotenv.2020.141614

Zhu, B., Alva, A.K., 1994. The effect of Gypsum amendment on transport of phosphorus in a sandy soil. Water. Air. Soil Pollut. 78, 375–382. https://doi.org/10.1007/BF00483044

Data availability

Water quality and quantity monitoring data from the Savijoki River used in this article: DOI: https://doi.org/10.48488/cpj7-wn62

Acknowledgements

This study was funded by the Ministry of Environment, Finland (Water protection programme), and by the Research Council of Finland (AnthroCliMocs-project 355018; Green-Digi Basin-project 347701). The fieldwork was carried out with the help of MSc Karoliina Lintunen (University of Turku, Finland), Linda Sainio and Vertti Markkanen.

SUOMEN MAANTIETEELLINEN SEURA